Theory of Light Scattering in Axion Electrodynamics

Tetsuyuki Ochiai

Photonic Materials Unit, National Institute for Materials Science (NIMS), Tsukuba, Ibaraki 305-0044, Japan

Taking account of the axion term in the Maxwell Lagrangian, we present a rigorous theory of light scattering in piecewise-constant axion fields. In particular, we focus on axionic substances with confined and/or curved geometries, and the scattering matrices of an axionic slab, cylinder, and sphere are derived analytically. The axion term generates a surface current with off-diagonal optical conductivity, giving rise to a new type of photospin-orbit interaction. As a result, various novel light-scattering phenomena can take place. We demonstrate enhanced Faraday rotation, parity-violating light scattering, and strong perturbation of dipole radiation.

KEYWORDS: axion, Mie scattering, S-matrix, topological insulator, Faraday rotation, dipole radiation

1. Introduction

Axion is a hypothetical particle used to explain the so-called strong CP (charge conjugation and parity) problem in elementary particle physics.[1] It is also a candidate for dark matter,[2] one of the biggest issues in physics and cosmology. Thus, many researchers have searched for axions with a great deal of effort. In the search for the axion, one of the key characteristics considered is its coupling with photons. This coupling is described by the so-called θ term (axion term) in the Lagrangian for a radiation field. Recently, this term has attracted growing interest in a very different context.

The θ term emerges in the effective theory for the radiation field in (strong) topological insulators.[3] This effective theory is described by the ordinary Maxwell Lagrangian plus the θ term, and is referred to as the axion electrodynamics.[4] The θ term is topological in the sense that it does not depend on the space-time metric. Actually, it is a total derivative, provided that the axion field is constant. Therefore, this term is negligible, at least locally in bulk, but has a non-negligible effect on a boundary. Thus, radiation dynamics in a topological insulator may have a non-negligible effect through the boundary surface. So far, most studies have assumed flat boundaries because planar crystal growth usually occurs. However, from the viewpoint of light scattering, the geometry of substances plays a crucial role. For instance, resonances and angular patterns depend strongly on the shape of the scatterer.

In this paper, we focus on the effects of confined and/or curved geometries in light scattering and discuss possible nontrivial phenomena induced by the θ term. In particular, we focus on three geometries: a slab of finite thickness, a circular cylinder, and a sphere. These are representative examples of confined and/or curved geometries and the analytic solution of light scattering can be obtained at $\theta = 0$. Moreover, by combining these geometries, complex geometries, such as a Bragg stack and a rough surface, can be studied. For instance, a rough surface is modeled as spheres placed on a slab. Therefore, to elucidate the role of the geometry in axion electrodynamics, the above three geometries are good examples. Interestingly enough, we show that even at nonzero θ, the analytic solution of light scattering in the three geometries can be obtained.

To be specific, the axion electrodynamics is defined by the following Lagrangian:

$$\mathcal{L} = \frac{1}{2}\boldsymbol{E}\cdot\boldsymbol{D} - \frac{1}{2}\boldsymbol{H}\cdot\boldsymbol{B} + \frac{e^2}{2\pi h}\theta\boldsymbol{E}\cdot\boldsymbol{B}. \tag{1}$$

Here, we assume a local and linear response of the polarization field, $\boldsymbol{D}(\boldsymbol{x},t) = \epsilon_0\epsilon(\boldsymbol{x})\boldsymbol{E}(\boldsymbol{x},t)$, and the magnetic permeability is set to be 1, $\boldsymbol{B}(\boldsymbol{x},t) = \mu_0\boldsymbol{H}(\boldsymbol{x},t)$. The third term in eq. (1) is the θ term, and $\theta = \theta(\boldsymbol{x},t)$ is called the axion field. The Euler-Lagrange equation becomes

$$\boldsymbol{\nabla}\cdot\boldsymbol{D} + \frac{c\epsilon_0\alpha}{\pi}\boldsymbol{\nabla}\theta\cdot\boldsymbol{B} = 0, \tag{2}$$

$$\boldsymbol{\nabla}\times\boldsymbol{H} - \frac{\partial\boldsymbol{D}}{\partial t} - \frac{c\epsilon_0\alpha}{\pi}\left(\frac{\partial\theta}{\partial t}\boldsymbol{B} + \boldsymbol{\nabla}\theta\times\boldsymbol{E}\right) = \boldsymbol{0}, \tag{3}$$

where $\alpha \equiv e^2/(4\pi\epsilon_0\hbar c)$ is the fine structure constant.

An axionic substance is characterized by a constant axion field, $\theta(\boldsymbol{x},t) = \theta_0$. Outside the substance, the axion field changes abruptly to 0. The abrupt change in the axion field generates a Hall current with off-diagonal conductivity $\sigma_H = \theta_0 e^2/(2\pi h)$. This Hall current on the boundary gives rise to nontrivial light scattering through the axionic substance. In particular, a new type of photospin-orbit interaction emerges and is different from the ordinary photospin-orbit interaction due to the quasi-transverse condition $\boldsymbol{\nabla}\cdot(\epsilon(\boldsymbol{x})\boldsymbol{E}) = 0$. Optical activity is a direct consequence of the new photospin-orbit interaction and has been discussed by several authors.[5–8] Here, we present further consequences of the photospin-orbit interaction, taking account of possible accumulation and the confined geometry of axionic substances. In particular, we demonstrate enhanced Faraday rotation, parity-violating light scattering, and strong perturbation in dipole radiation.

This paper is organized as follows. In §2 we investigate the scattering (S) matrix of axionic substances by assuming rather simple geometries. Section 3 is devoted to present the enhanced Faraday rotation in a Bragg stack of axionic slabs. In §4 parity-violating light scattering in an axionic cylinder is demonstrated. The strong perturbation of dipole radiation in an axionic sphere is shown in §5. Finally, a summary and discussion are given in §6.

2. Scattering Matrix of Axionic Substance

In what follows, we consider light scattering by axionic substances with rather simple geometries. The key quantity

in light scattering is the S-matrix, which relates the amplitude of the incoming wave to that of the outgoing wave. Once we have the S-matrix, we can solve various types of light-scattering problems in isolated axionic substances. Moreover, by employing the multiple-scattering formalism, we can deal with composite systems of axionic substances. The interaction among axionic substances may enhance nontrivial effects that are favorable for experimental detection.

To derive the S-matrix, the boundary condition of the electromagnetic field is crucial. The boundary condition in axion electrodynamics is given by

$$\Delta D_\perp = -\frac{c\epsilon_0\alpha\theta_0}{\pi}B_\perp, \tag{4}$$

$$\Delta B_\perp = 0, \tag{5}$$

$$\Delta \boldsymbol{E}_\parallel = \boldsymbol{0}, \tag{6}$$

$$\Delta \boldsymbol{H}_\parallel = \frac{c\epsilon_0\alpha\theta_0}{\pi}\boldsymbol{E}_\parallel, \tag{7}$$

Here, subscripts $\parallel$ and $\perp$ respectively stand for parallel and perpendicular components with respect to the boundary surface, $\Delta\boldsymbol{F} \equiv \boldsymbol{F}(x_\perp = \delta) - \boldsymbol{F}(x_\perp = -\delta)$ is the discontinuity at boundary (δ is an infinitesimal positive number), and the axion field changes abruptly from 0 ($x_\perp < 0$) to θ_0 ($x_\perp > 0$). Away from the boundary surface, the radiation field satisfies the Helmholtz equation because $\epsilon(\boldsymbol{x})$ is piecewise constant. Thus, it is easy to write down the incoming and outgoing fields of the transverse wave. With the boundary condition, the connection between the incoming and outgoing waves is given. This connection defines the S-matrix.

It is worth noting that the above boundary condition is equivalent to that in the case of surface charge and current. In this case, the boundary condition on the xy plane becomes

$$\Delta D_z = \rho^{\mathrm{2d}}, \tag{8}$$

$$\Delta H_x = j_y^{\mathrm{2d}}, \tag{9}$$

$$\Delta H_y = -j_x^{\mathrm{2d}}, \tag{10}$$

and the remainder of the boundary condition is the same. Therefore, the abrupt change in the axion field induces the surface charge and current, from which the Hall conductance of $\sigma_H = \theta_0 e^2/(2\pi h)$ is derived. Further discussion about the boundary condition is given in §6.

2.1 Slab

First, let us consider the S-matrix of an axionic slab sandwiched by normal substances. The slab is assumed to have infinite extent in the xy direction and to have finite thickness d. The permittivity ϵ_a and constant axion field θ_0 are attributed to the slab. The upper (lower) medium has permittivity $\epsilon_u(\epsilon_l)$. The S-matrix relates the incoming wave to the outgoing waves as

$$\begin{pmatrix} a_u^\beta \\ b_l^\beta \end{pmatrix} = \sum_{\beta'=P,S}\begin{pmatrix} S_{++}^{\beta\beta'} & S_{+-}^{\beta\beta'} \\ S_{-+}^{\beta\beta'} & S_{--}^{\beta\beta'} \end{pmatrix}\begin{pmatrix} a_l^{\beta'} \\ b_u^{\beta'} \end{pmatrix}, \tag{11}$$

where $a_u^\beta, b_u^\beta, a_l^\beta, b_l^\beta$ ($\beta = P, S$) are the coefficients of the plane waves with P and S polarizations:

$$\boldsymbol{E}^\sigma(\boldsymbol{x}) = (a_\sigma^P\hat{\boldsymbol{p}}_\sigma^+ + a_\sigma^S\hat{\boldsymbol{s}})\mathrm{e}^{\mathrm{i}\boldsymbol{K}_\sigma^+\cdot\boldsymbol{x}} + (b_\sigma^P\hat{\boldsymbol{p}}_\sigma^- + b_\sigma^S\hat{\boldsymbol{s}})\mathrm{e}^{\mathrm{i}\boldsymbol{K}_\sigma^-\cdot\boldsymbol{x}}, \tag{12}$$

$$\boldsymbol{K}_\sigma^\pm = \boldsymbol{k}_\parallel \pm \gamma_\sigma\hat{z}, \quad \gamma_\sigma = \sqrt{q_\sigma^2 - \boldsymbol{k}_\parallel^2}, \quad q_\sigma = \frac{\omega}{c}\sqrt{\epsilon_\sigma}, \tag{13}$$

$$\hat{\boldsymbol{p}}_\sigma^\pm = \pm\frac{\gamma_\sigma}{q_\sigma}\hat{\boldsymbol{k}}_\parallel - \frac{|\boldsymbol{k}_\parallel|}{q_\sigma}\hat{z}, \quad \hat{\boldsymbol{s}} = \hat{\boldsymbol{k}}_\perp, \tag{14}$$

$$\hat{\boldsymbol{k}}_\parallel = \frac{1}{|\boldsymbol{k}_\parallel|}(k_x, k_y), \quad \hat{\boldsymbol{k}}_\perp = \frac{1}{|\boldsymbol{k}_\parallel|}(-k_y, k_x), \tag{15}$$

for $\sigma = u, l$. Here, $\boldsymbol{E}^{u(l)}$ is the electric field in the upper (lower) medium. Since the system has translational invariance in the xy direction, the wave vector $\boldsymbol{k}_\parallel$ parallel to the slab surfaces is conserved.

To construct the S-matrix of the slab, it is convenient to introduce the S-matrix of a flat interface between axionic ($z > 0$) and normal ($z < 0$) substances. Suppose that the normal substance has permittivity ϵ_b. The interface S-matrix becomes

$$[S_{++}] = 2\gamma_b[A]^{-1}, \qquad [S_{+-}] = [A]^{-1}[B],$$
$$[S_{-+}] = -([A]^t)^{-1}[B]^t, \quad [S_{--}] = 2\gamma_a([A]^t)^{-1}, \tag{16}$$

$$[A] = \begin{pmatrix} \frac{q_b}{q_a}\gamma_a + \frac{q_a}{q_b}\gamma_b & -\frac{\alpha\theta_0\omega}{\pi c}\frac{\gamma_b}{q_b} \\ \frac{\alpha\theta_0\omega}{\pi c}\frac{\gamma_a}{q_a} & \gamma_a + \gamma_b \end{pmatrix}, \tag{17}$$

$$[B] = \begin{pmatrix} \frac{q_b}{q_a}\gamma_a - \frac{q_a}{q_b}\gamma_b & \frac{\alpha\theta_0\omega}{\pi c}\frac{\gamma_b}{q_b} \\ \frac{\alpha\theta_0\omega}{\pi c}\frac{\gamma_a}{q_a} & \gamma_a - \gamma_b \end{pmatrix}. \tag{18}$$

Here, $q_a, q_b, \gamma_a, \gamma_b$ are defined as in eq. (13), and we employ the matrix notation

$$[X] \equiv \begin{pmatrix} X^{PP} & X^{PS} \\ X^{SP} & X^{SS} \end{pmatrix}, \quad X = S_{\pm\pm}, A, B. \tag{19}$$

Of particular importance is the mixing between P and S polarizations, which vanishes at $\theta_0 = 0$. This mixing induces Faraday and Kerr rotations through the interface, in which the rotation angle is of order α. At $\theta_0 = 0$, P and S polarizations are decoupled. This decoupling is a consequence of the ordinary photospin-orbit interaction, which lifts the degeneracy between P and S, and of the in-plane symmetry, which prohibits the coupling between P and S. At finite θ_0, P and S polarizations are then mixed through the boundary condition of the electromagnetic (orbital) field. Therefore, this mixing represents a new class of photospin-orbit interaction other than the ordinary interaction, that caused by the magneto-optical effect, and that caused by chirality.[9] This point is further clarified in §6.

For the case of a slab with two parallel interfaces, we need to know the S-matrix of the lower ($z = -d/2$) and upper ($z = d/2$) interfaces. The S-matrix of the lower interface is obtained from eq. (16) by replacing ϵ_b with ϵ_l. For the upper interface, the S-matrix is obtained by replacing $(\epsilon_a, \epsilon_b, \theta_0)$ with $(\epsilon_u, \epsilon_a, -\theta_0)$. The slab S-matrix is obtained in a layer-by-layer manner[10] as

$$[S_{++}] = \tilde{S}^u_{++}(1 - \tilde{S}^l_{+-}\tilde{S}^u_{-+})^{-1}\tilde{S}^l_{++},$$
$$[S_{+-}] = \tilde{S}^u_{+-} + \tilde{S}^u_{++}(1 - \tilde{S}^l_{+-}\tilde{S}^u_{-+})^{-1}\tilde{S}^l_{+-}\tilde{S}^u_{--},$$
$$[S_{-+}] = \tilde{S}^l_{-+} + \tilde{S}^l_{--}(1 - \tilde{S}^u_{-+}\tilde{S}^l_{+-})^{-1}\tilde{S}^u_{-+}\tilde{S}^l_{++},$$
$$[S_{--}] = \tilde{S}^l_{--}(1 - \tilde{S}^u_{-+}\tilde{S}^l_{+-})^{-1}\tilde{S}^u_{--}, \tag{20}$$

$$\begin{pmatrix} \tilde{S}^u_{++} & \tilde{S}^u_{+-} \\ \tilde{S}^u_{-+} & \tilde{S}^u_{--} \end{pmatrix} = \begin{pmatrix} \mathrm{e}^{\mathrm{i}(\gamma_a-\gamma_u)\frac{d}{2}}S^u_{++} & \mathrm{e}^{-\mathrm{i}\gamma_u d}S^u_{+-} \\ \mathrm{e}^{\mathrm{i}\gamma_a d}S^u_{-+} & \mathrm{e}^{\mathrm{i}(\gamma_a-\gamma_u)\frac{d}{2}}S^u_{--} \end{pmatrix}, \tag{21}$$

$$\begin{pmatrix} \tilde{S}^{\,l}_{++} & \tilde{S}^{\,l}_{+-} \\ \tilde{S}^{\,l}_{-+} & \tilde{S}^{\,l}_{--} \end{pmatrix} = \begin{pmatrix} \mathrm{e}^{\mathrm{i}(\gamma_a-\gamma_l)\frac{d}{2}} S^{\,l}_{++} & \mathrm{e}^{\mathrm{i}\gamma_a d} S^{\,l}_{+-} \\ \mathrm{e}^{-\mathrm{i}\gamma_l d} S^{\,l}_{-+} & \mathrm{e}^{\mathrm{i}(\gamma_a-\gamma_l)\frac{d}{2}} S^{\,l}_{--} \end{pmatrix}, \quad (22)$$

where the matrix notation is omitted on the right-hand side of eq. (20).

2.2 Cylinder

Next, we consider an axionic cylinder of infinite length and circular cross section. The cylinder has radius r_a, permittivity ϵ_a, and constant axion field θ_0. The background medium has permittivity ϵ_b. Owing to the translational invariance along the cylindrical axis (z axis), a wave vector parallel to the axis is conserved. Thus, inside and outside the cylinder, the electric field can be expanded in terms of the M and N polarization basis as[11]

$$\boldsymbol{E}^{\sigma}(\boldsymbol{x}) = \boldsymbol{E}^{\sigma J}(\boldsymbol{x}) + \boldsymbol{E}^{\sigma H}(\boldsymbol{x}), \quad (23)$$

$$\boldsymbol{E}^{\sigma Z}(\boldsymbol{x}) = -\frac{1}{\lambda_\sigma}\hat{z}\times\boldsymbol{\nabla}\psi^{M\sigma Z}(\boldsymbol{x}) + \left(\frac{\mathrm{i}k_z}{\lambda_\sigma q_\sigma}\boldsymbol{\nabla}_\parallel + \frac{\lambda_\sigma}{q_\sigma}\hat{z}\right)\psi^{N\sigma Z}(\boldsymbol{x}), \quad (24)$$

$$\psi^{\beta\sigma Z}(\boldsymbol{x}) = \sum_{n\in\boldsymbol{Z}} Z_n(\lambda_\sigma\rho)\mathrm{e}^{\mathrm{i}n\phi}\mathrm{e}^{\mathrm{i}k_z z}\psi_n^{\beta\sigma Z}, \quad (25)$$

$$\lambda_\sigma = \sqrt{q_\sigma^2 - k_z^2}, \quad (26)$$

for $Z = J, H$, $\sigma = a, b$, and $\beta = M, N$. Here, $\boldsymbol{E}^{a(b)}$ is the electric field inside (outside) the sphere, J_n is the nth order Bessel function, H_n is the nth order Hankel function of the first kind, and (ρ, ϕ, z) are the cylindrical coordinates. The terms M and N polarizations refer to the two independent transverse modes of the vector cylindrical wave. The M and N polarizations correspond to the S and P polarizations, respectively, if we define the incident plane as that formed by the cylindrical axis and the incident $\boldsymbol{k}$ vector.

The S-matrix of the cylinder surface is defined by

$$\begin{pmatrix} \psi_n^{\beta aJ} \\ \psi_n^{\beta bH} \end{pmatrix} = \sum_{\beta'=M,N} \begin{pmatrix} S^{\beta\beta'}_{n++} & S^{\beta\beta'}_{n+-} \\ S^{\beta\beta'}_{n-+} & S^{\beta\beta'}_{n--} \end{pmatrix} \begin{pmatrix} \psi_n^{\beta' bJ} \\ \psi_n^{\beta' aH} \end{pmatrix}. \quad (27)$$

By imposing the boundary condition on the cylindrical surface, we can obtain the analytic expression for the S-matrix as

$$[S_{n++}] = -\frac{2\mathrm{i}}{\pi}[A_n]^{-1}, \qquad [S_{n+-}] = -[A_n]^{-1}[B_n],$$

$$[S_{n-+}] = -[C_n]^{-1}[D_n], \quad [S_{n--}] = -\frac{2\mathrm{i}}{\pi}[C_n]^{-1}, \quad (28)$$

$$[A_n] = [d_n^{<}] - \frac{\mathrm{i}\alpha\theta_0}{\pi}\begin{pmatrix} 0 & -\frac{\omega}{cq_a}\xi_a J_n(\xi_a)H_n'(\xi_b) \\ \frac{\omega}{cq_b}\xi_b J_n'(\xi_a)H_n(\xi_b) & \frac{nk_z\omega}{cq_aq_b}\left(\frac{\xi_b}{\xi_a}-\frac{\xi_a}{\xi_b}\right)J_n(\xi_a)H_n(\xi_b) \end{pmatrix}, \quad (29)$$

$$[B_n] = [d_n^{H>}] - \frac{\mathrm{i}\alpha\theta_0}{\pi}\begin{pmatrix} 0 & -\frac{\omega}{cq_a}\xi_a H_n(\xi_a)H_n'(\xi_b) \\ \frac{\omega}{cq_b}\xi_b H_n'(\xi_a)H_n(\xi_b) & \frac{nk_z\omega}{cq_aq_b}\left(\frac{\xi_b}{\xi_a}-\frac{\xi_a}{\xi_b}\right)H_n(\xi_a)H_n(\xi_b) \end{pmatrix}, \quad (30)$$

$$[C_n] = [d_n^{<}]^t - \frac{\mathrm{i}\alpha\theta_0}{\pi}\begin{pmatrix} 0 & -\frac{\omega}{cq_b}\xi_b J_n'(\xi_a)H_n(\xi_b) \\ \frac{\omega}{cq_a}\xi_a J_n(\xi_a)H_n'(\xi_b) & -\frac{nk_z\omega}{cq_aq_b}\left(\frac{\xi_b}{\xi_a}-\frac{\xi_a}{\xi_b}\right)J_n(\xi_a)H_n(\xi_b) \end{pmatrix}, \quad (31)$$

$$[D_n] = [d_n^{J>}]^t - \frac{\mathrm{i}\alpha\theta_0}{\pi}\begin{pmatrix} 0 & -\frac{\omega}{cq_b}\xi_b J_n'(\xi_a)J_n(\xi_b) \\ \frac{\omega}{cq_a}\xi_a J_n(\xi_a)J_n'(\xi_b) & -\frac{nk_z\omega}{cq_aq_b}\left(\frac{\xi_b}{\xi_a}-\frac{\xi_a}{\xi_b}\right)J_n(\xi_a)J_n(\xi_b) \end{pmatrix}, \quad (32)$$

$$[d_n^{<}] = \begin{pmatrix} \xi_b J_n'(\xi_a)H_n(\xi_b) - \xi_a J_n(\xi_a)H_n'(\xi_b) & \frac{nk_z}{q_a}\left(\frac{\xi_b}{\xi_a}-\frac{\xi_a}{\xi_b}\right)J_n(\xi_a)H_n(\xi_b) \\ \frac{nk_z}{q_b}\left(\frac{\xi_b}{\xi_a}-\frac{\xi_a}{\xi_b}\right)J_n(\xi_a)H_n(\xi_b) & \frac{q_a}{q_b}\xi_b J_n'(\xi_a)H_n(\xi_b) - \frac{q_b}{q_a}\xi_a J_n(\xi_a)H_n'(\xi_b) \end{pmatrix}, \quad (33)$$

$$[d_n^{Z>}] = \begin{pmatrix} \xi_b Z_n'(\xi_a)Z_n(\xi_b) - \xi_a Z_n(\xi_a)Z_n'(\xi_b) & \frac{nk_z}{q_a}\left(\frac{\xi_b}{\xi_a}-\frac{\xi_a}{\xi_b}\right)Z_n(\xi_a)Z_n(\xi_b) \\ \frac{nk_z}{q_b}\left(\frac{\xi_b}{\xi_a}-\frac{\xi_a}{\xi_b}\right)Z_n(\xi_a)Z_n(\xi_b) & \frac{q_a}{q_b}\xi_b Z_n'(\xi_a)Z_n(\xi_b) - \frac{q_b}{q_a}\xi_a Z_n(\xi_a)Z_n'(\xi_b) \end{pmatrix}, \quad (34)$$

where $\xi_\sigma \equiv \lambda_\sigma r_a$ ($\sigma = a, b$) and the matrix notation

$$[X] = \begin{pmatrix} X^{MM} & X^{MN} \\ X^{NM} & X^{NN} \end{pmatrix} \quad (35)$$

is employed for $X = S_{n\pm\pm}, A_n, B_n, C_n, D_n$.

At $\theta_0 = 0$, M and N polarizations are decoupled if $k_z = 0$. This decoupling is again a consequence of the photospin-orbit interaction and the inversion symmetry under $z \to -z$. If $k_z \neq 0$, the two polarizations are mixed even at $\theta_0 = 0$. However, this mixing is different from that at finite θ_0, because the parity with respect to a plane including the cylindrical axis is preserved at $\theta_0 = 0$. With the latter mixing, this parity is broken. We will see this effect in §4.

2.3 Sphere

Another analytic solution can be obtained for an axionic sphere. Suppose that the sphere has radius r_a, permittivity ϵ_a, and constant axion field θ_0. The background medium has permittivity ϵ_b. The electric field inside and outside the sphere is

expressed in terms of the M and N polarization basis as[12,13]

$$\boldsymbol{E}^{\sigma}(\boldsymbol{x}) = \boldsymbol{E}^{\sigma j}(\boldsymbol{x}) + \boldsymbol{E}^{\sigma h}(\boldsymbol{x}), \tag{36}$$

$$\boldsymbol{E}^{\sigma z}(\boldsymbol{x}) = \mathrm{i}\boldsymbol{L}\psi^{M\sigma z} + \frac{1}{q_\sigma}\boldsymbol{\nabla}\times\mathrm{i}\boldsymbol{L}\psi^{N\sigma z}, \tag{37}$$

$$\psi^{\beta\sigma z}(\boldsymbol{x}) = \sum_L z_l(q_\sigma r)Y_L(\hat{\boldsymbol{x}})\psi_L^{\beta\sigma z}, \tag{38}$$

for $z = j, h$, $\sigma = a, b$, and $\beta = M, N$. Here, $\boldsymbol{L} \equiv -\mathrm{i}\boldsymbol{x}\times\boldsymbol{\nabla}$, j_l is the lth order spherical Bessel function, h_l is the lth order spherical Hankel function of the first kind, $Y_L(\hat{\boldsymbol{x}})$ is the spherical harmonics, and $L = (l, m)$ is the three-dimensional angular momentum with $-l \le m \le l$.

The S-matrix of the spherical surface is then defined by

$$\begin{pmatrix} \psi_L^{\beta a j} \\ \psi_L^{\beta b h} \end{pmatrix} = \sum_{\beta'=M,N} \begin{pmatrix} S_{l++}^{\beta\beta'} & S_{l+-}^{\beta\beta'} \\ S_{l-+}^{\beta\beta'} & S_{l--}^{\beta\beta'} \end{pmatrix} \begin{pmatrix} \psi_L^{\beta' b j} \\ \psi_L^{\beta' a h} \end{pmatrix}. \tag{39}$$

Because of the rotational invariance of the system, the S-matrix is diagonal with respect to L and does not depend on m. By imposing the boundary condition, we obtain

$$[S_{l++}] = -\frac{\mathrm{i}}{\rho_b}[A_l]^{-1}, \qquad [S_{l+-}] = -[A_l]^{-1}[B_l],$$

$$[S_{l-+}] = -[C_l]^{-1}[D_l], \quad [S_{l--}] = -\frac{\mathrm{i}}{\rho_a}[C_l]^{-1}, \tag{40}$$

$$[A_l] = \begin{pmatrix} d_l^{<} & -\frac{\mathrm{i}\alpha\theta_0}{\pi}\frac{\omega}{c}r_0\frac{(\rho_a j_l(\rho_a))'}{\rho_a}h_l(\rho_b) \\ \frac{\mathrm{i}\alpha\theta_0}{\pi}\frac{\omega}{c}r_0 j_l(\rho_a)\frac{(\rho_b h_l(\rho_b))'}{\rho_b} & w_l^{<} \end{pmatrix}, \tag{41}$$

$$[B_l] = \begin{pmatrix} d_l^{h>} & -\frac{\mathrm{i}\alpha\theta_0}{\pi}\frac{\omega}{c}r_0\frac{(\rho_a h_l(\rho_a))'}{\rho_a}h_l(\rho_b) \\ \frac{\mathrm{i}\alpha\theta_0}{\pi}\frac{\omega}{c}r_0 h_l(\rho_a)\frac{(\rho_b h_l(\rho_b))'}{\rho_b} & w_l^{h>} \end{pmatrix}, \tag{42}$$

$$[C_l] = \begin{pmatrix} d_l^{<} & -\frac{\mathrm{i}\alpha\theta_0}{\pi}\frac{\omega}{c}r_0 j_l(\rho_a)\frac{(\rho_b h_l(\rho_b))'}{\rho_b} \\ \frac{\mathrm{i}\alpha\theta_0}{\pi}\frac{\omega}{c}r_0\frac{(\rho_a j_l(\rho_a))'}{\rho_a}h_l(\rho_b) & w_l^{<} \end{pmatrix}, \tag{43}$$

$$[D_l] = \begin{pmatrix} d_l^{j>} & -\frac{\mathrm{i}\alpha\theta_0}{\pi}\frac{\omega}{c}r_0 j_l(\rho_a)\frac{(\rho_b j_l(\rho_b))'}{\rho_b} \\ \frac{\mathrm{i}\alpha\theta_0}{\pi}\frac{\omega}{c}r_0\frac{(\rho_a j_l(\rho_a))'}{\rho_a}j_l(\rho_b) & w_l^{j>}, \end{pmatrix}, \tag{44}$$

$$d_l^{<} = \rho_a j_l'(\rho_a)h_l(\rho_b) - \rho_b j_l(\rho_a)h_l'(\rho_b), \tag{45}$$

$$d_l^{z>} = \rho_a z_l'(\rho_a)z_l(\rho_b) - \rho_b z_l(\rho_a)z_l'(\rho_b), \tag{46}$$

$$w_l^{<} = \frac{\rho_b}{\rho_a}(\rho_a j_l(\rho_a))'h_l(\rho_b) - \frac{\rho_a}{\rho_b}j_l(\rho_a)(\rho_b h_l(\rho_b))', \tag{47}$$

$$w_l^{z>} = \frac{\rho_b}{\rho_a}(\rho_a z_l(\rho_a))'z_l(\rho_b) - \frac{\rho_a}{\rho_b}z_l(\rho_a)(\rho_b z_l(\rho_b))', \tag{48}$$

where $\rho_\sigma \equiv q_\sigma r_a$ ($\sigma = a, b$).

3. Faraday Rotation in Stacked Axionic Slabs

A vivid example that illustrates the role of the θ term is the Faraday and Kerr rotations of polarized light. This effect was studied by several authors, and the rotation angle of the Faraday rotation is generally small. To enhance the polarization rotation angle, we consider a Bragg stack of axionic slabs. The optical properties of the Bragg stack can be described by the S-matrix, which can be numerically obtained in a layer-by-layer manner, from the S-matrix of an isolated axionic slab. In a Bragg stack composed of ordinary media, the P and S polarizations are decoupled, and the resulting photonic bands are either P- or S-polarized. Thus, no polarization rotation takes place as long as the incident wave is either P- or S-polarized. However, if θ_0 is finite, the P and S polarizations are mixed, forming mixed photonic bands with (incident) angle-dependent stop bands.

As an example, let us consider an incident wave of S-polarization with Brewster angle $\theta_B \equiv \tan^{-1}(\sqrt{\epsilon_a/\epsilon_b})$. A schematic illustration of the system under study is shown in Fig. 1. Strictly speaking, in our case antireflection takes place for nonpurely P polarized light at an incident angle slightly shifted from θ_B. However, the system still almost shows antireflection. Figure 2 shows the photonic band structure, transmittance, Faraday rotation and ellipticity spectra in an axionic Bragg stack. The Bragg stack is composed of eight axionic slabs placed periodically in air. The photonic band diagram consists of two kinds of dispersion curves, straight and curved ones. The former correspond to P-like bands with gapless dispersion owing to the anti-reflection. The latter are S-like bands with gapped dispersion. The S-polarized incident light mostly excites the S-like band modes. Therefore, the transmission spectrum exhibits Fabri-Perot resonances in the S-like band regions and dips in the gap region of the S-like bands. We stress that the transmittance still shows finite val-

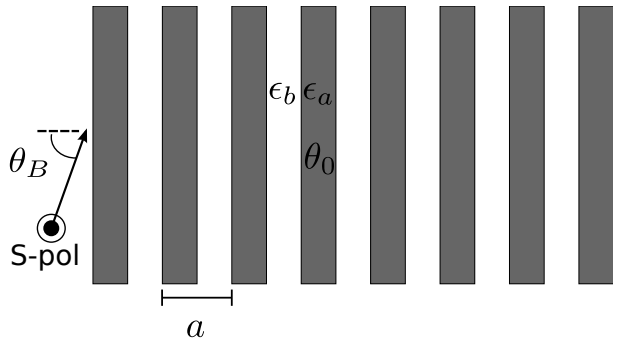

Fig. 1. Schematic illustration of the Bragg stack under study. Axionic slabs of permittivity ϵ_a and constant axion field θ_0 are aligned periodically with lattice constant a in a background medium of permittivity ϵ_b. The S-polarized light is incident on the Bragg stack with Brewster angle θ_B.

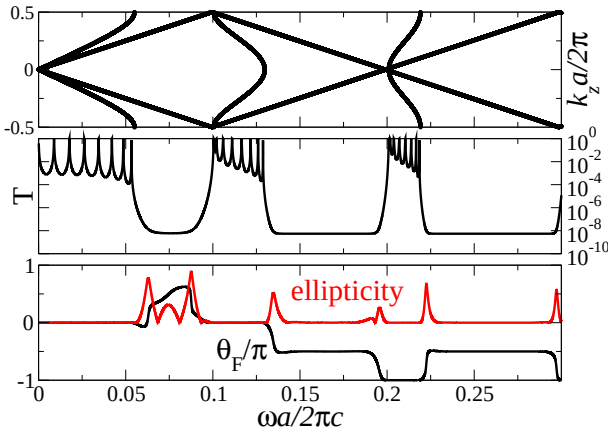

Fig. 2. (Color online) Photonic band structure, transmittance (T), Faraday rotation (θ_F), and ellipticity of the transmitted light in the axionic Bragg stack. Eight axionic slabs of $\epsilon_a = 100$ and $\theta_0 = \pi$ (taken from ref.[5] for Bi_2Se_3) are aligned periodically in air ($\epsilon_b = 1$). The slab thickness is taken to be $0.5a$.

ues of order 10^{-8} in the gap. These small values are due to the mixing between P and S polarizations, and the P-like component of the incident S-polarized light can transmit through the Bragg stack. This transmission gives rise to an enhanced Faraday rotation. We should note that at $\theta_0 = 0$, the dip becomes deeper with increasing number of slabs, whereas the transmittance in the dip does not change significantly at finite θ_0.

As expected, the Faraday rotation angle is nearly $\pm\pi/2$ (P-polarized) in the S-gap region and nearly an integer multiple of π (S-polarized) otherwise. The transmitted light is, in general, elliptically polarized because of the mixing between P and S polarizations and because of their phase difference. The ellipticity is enhanced near the stop-band edges.

4. Parity-Violating Light Scattering by Axionic Cylinder

Next, let us consider a plane wave of wave vector $\boldsymbol{k}$ and polarization $\boldsymbol{p}$ incident on an axionic cylinder. In this case, the multipole component of the incident wave is expressed as eq. (25) with

$$\psi_n^{MbJ} = \mathrm{i}^n \mathrm{e}^{-\mathrm{i}n\phi(\boldsymbol{k})}\left(-\frac{1}{2}p_- \mathrm{e}^{\mathrm{i}\phi(\boldsymbol{k})} + \frac{1}{2}p_+ \mathrm{e}^{-\mathrm{i}\phi(\boldsymbol{k})}\right),$$

$$\psi_n^{NbJ} = \mathrm{i}^n \mathrm{e}^{-\mathrm{i}n\phi(\boldsymbol{k})}\left(-\frac{k_z}{2q_b}(p_- \mathrm{e}^{\mathrm{i}\phi(\boldsymbol{k})} + p_+ \mathrm{e}^{-\mathrm{i}\phi(\boldsymbol{k})}) + \frac{\lambda_b}{q_b}p_z\right),$$

$$\psi_n^{MaH} = \psi_n^{NaH} = 0, \tag{49}$$

where $p_\pm \equiv p_x \pm \mathrm{i}p_y$. The $P(S)$ polarization gives $\psi^{MbJ} = 0$ ($\psi^{NbJ} = 0$) (here, the incident plane is defined by the plane formed by the incident wave vector and the cylindrical axis). The scattering cross section of the cylinder per unit length is written as

$$\sigma_{\mathrm{tot}} = \int_0^{2\pi} \mathrm{d}\phi \sigma_{\mathrm{dcs}}(\phi), \tag{50}$$

$$\sigma_{\mathrm{dcs}}(\phi) = \sum_{\beta=M,N} |f^\beta(\phi)|^2, \tag{51}$$

$$f^\beta(\phi) = \sqrt{\frac{2}{\pi\lambda_b}} \sum_n (-\mathrm{i})^{n+1} \mathrm{e}^{\mathrm{i}n\phi} \psi_n^{\beta bH}. \tag{52}$$

Let us set $\phi(\boldsymbol{k}) = 0$. Then, the incident wave is expressed as $\boldsymbol{E}^{\mathrm{inc}} = \boldsymbol{p}\exp(\mathrm{i}k_x x + \mathrm{i}k_z z)$, and it is obvious that the incident wave of P and S polarizations is either symmetric or antisymmetric under $y \to -y$ ($\phi \to -\phi$). As a result, the differential cross section $\sigma_{\mathrm{dcs}}(\phi)$ becomes symmetric under $\phi \to -\phi$ in the ordinary case. The presence of the θ term violates this symmetry, and the resulting cross section exhibits an asymmetric distribution. We express the degree of the asymmetry as

$$AS(\phi) \equiv \left|\frac{\sigma_{\mathrm{dcs}}(\phi) - \sigma_{\mathrm{dcs}}(-\phi)}{\sigma_{\mathrm{dcs}}(\phi)}\right|. \tag{53}$$

Figure 3 shows the total cross section σ_{tot} for P- and S-polarized light as a function of frequency, the differential cross section $\sigma_{\mathrm{dcs}}(\phi)$ for P-polarized light at a resonant frequency, and the degree of asymmetry $AS(\phi)$ at the same frequency. An oblique incidence of 30° is assumed. The total cross section exhibits a series of Mie resonances whose polarization properties are not purely P- and S-polarized. This mixing takes place even if $\theta_0 = 0$. Let us focus on the resonance at $\omega a/2\pi c = 0.1213$ for the P-polarized incident light. This resonance has angular momentum $n = 2$ and is close in frequency to the resonance at $\omega a/2\pi c = 0.121$ for the S-polarized incident light. This resonance has angular momentum $n = 1$. The angular distribution of the former resonance approximately exhibits a $2n$-fold rotational symmetric pattern, because the angular momenta of both n and $-n$ contribute to $f^\beta(\phi)$. We should point out that the angular distribution has a slight deviation from the symmetric configuration with respect to $\phi = 0$, although it seems to be symmetric. In fact, the degree of asymmetry becomes nonzero and shows a complex profile owing to the overlap between the two resonances with different angular momenta. This asymmetry results from the strong perturbation of the θ term, which is affected by the resonance nearby. As in the degenerate perturbation, the perturbation of the lowest order in α can survive in the differential cross section, giving rise to enhanced asymmetry. In this way, the light scattering by an axionic cylinder is parity-violating.

An important ingredient of the parity violation is the oblique incidence. In the normal incident case, the parity invariance is recovered. This property originates from the symmetry of the S-matrix under the inversion of the angular mo-

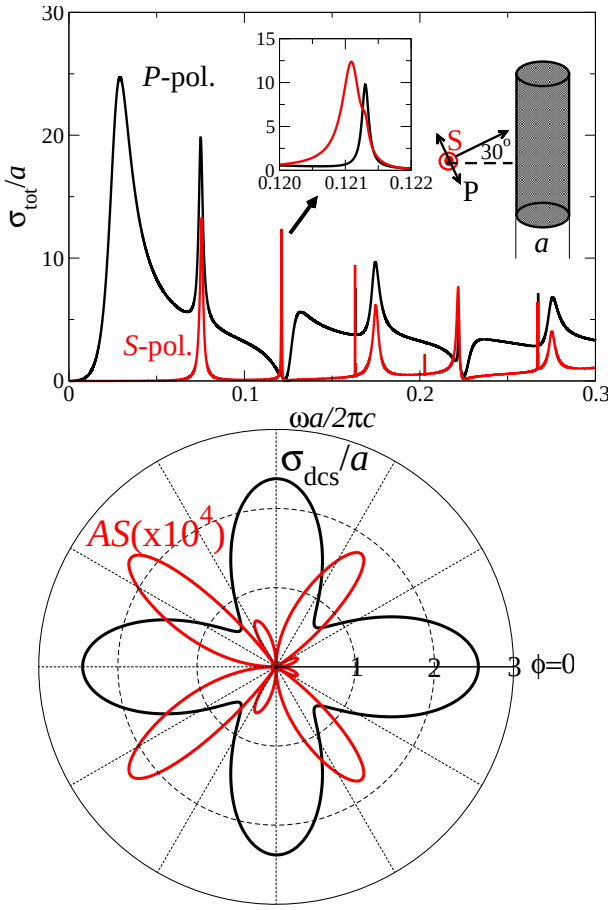

Fig. 3. (Color online) Scattering cross sections of the axionic cylinder with $\epsilon_a = 100$, $\theta_0 = \pi$, and diameter a in air. The plane wave is incident on the cylinder with an incident angle of 30°. (Upper panel) Total cross section as a function of frequency. Both P- and S-polarized incident light are considered. (Lower panel) Differential cross section and degree of asymmetry at resonance frequency of $\omega a/2\pi c = 0.1213$ for P-polarized incident light. The incident azimuthal angle is 0°.

mentum n. At $\theta_0 = 0$, this symmetry becomes

$$[X_{-n}] = \begin{pmatrix} X_n^{MM} & -X_n^{MN} \\ -X_n^{NM} & X_n^{NN} \end{pmatrix}, \; X = S_{\pm\pm}, A, B, C, D. \quad (54)$$

We should note that the off-diagonal terms X_n^{MN} and X_n^{MN} vanish if $k_z = 0$, resulting in the decoupling of P and S polarizations. Therefore, for the P-polarized incident light, for instance, we can show that $f^M(-\phi) = -f^M(\phi)$ and $f^N(-\phi) = f^N(\phi)$, resulting in $\sigma_{\rm dcs}(-\phi) = \sigma_{\rm dcs}(\phi)$. At finite θ_0, this symmetry is broken. However, if $k_z = 0$, the symmetry is recovered as $[X_{-n}] = [X_n]$ irrespective of θ_0. In this case, we can prove that $f^\beta(-\phi) = f^\beta(\phi)$ ($\beta = M, N$). Again we have $\sigma_{\rm dcs}(-\phi) = \sigma_{\rm dcs}(\phi)$. Thus, the degree of asymmetry is zero for the normal incidence.

Let me comment on experimental aspects of parity-violating light scattering. To observe parity-violating signals, it is important that the specimen has parity symmetry in its shape. This condition does not exclude a cylinder with a rectangular cross section, which is more easily fabricated than a cylinder with a circular cross section. Light scattering by a rectangular cylinder can be described by an S-matrix that is not diagonal with respect to angular momentum index n.

5. Strong Perturbation of Dipole Radiation in Axionic Sphere

As a final example, let us consider an oscillating dipole placed inside an axionic sphere. The multipole component of the incident wave induced by the oscillating dipole is expressed as eq. (38) with the following multipole components:

$$\psi_L^{\beta bj} = 0,$$

$$\psi_L^{\beta ah} = \frac{i\mu_0\omega^2 q_a}{l(l+1)} \sum_{L'} \boldsymbol{d} \cdot [(\boldsymbol{P}^\beta)^\dagger]_{LL'} j_{l'}(q_a r_0) Y^*_{L'}(\hat{\boldsymbol{x}}_0), \quad (55)$$

where $\boldsymbol{d}$ is the electric dipole moment, $\boldsymbol{x}_0$ is the dipole position inside the sphere, and matrix $\boldsymbol{P}^\beta$ is the vector-spherical-wave expansion coefficient. For its expression, please consult the appendix. We should note that $[\boldsymbol{P}^M]_{LL'}$ is diagonal with respect to index l. Therefore, $\psi_L^{Mah} = 0$ for a particular angular momentum l irrespective of m, provided that $q_a r_0 = j_{l+\frac{1}{2},n}$, i.e., the nth zero of the spherical Bessel function of order l.

Moreover, at $\theta_0 = 0$, the Mie resonance is classified according to β, l, and the principal number n. At the resonant frequencies, we have $d_l^< \simeq 0$ ($w_l^< \simeq 0$) for $\beta = M(N)$. This property along with the vanishing multipole component implies that the Mie resonance of $\beta = M(N)$ with angular momentum l becomes hidden if $q_a r_0 = j_{l+\frac{1}{2},n}$ is satisfied at the resonant frequency.

On the other hand, at finite θ_0, the Mie resonance is not simply classified according to polarization β. Instead, at resonance frequencies we have

$$d_l^< w_l^< \simeq \left(\frac{\alpha\theta_0}{\pi}\frac{\omega}{c}r_0\right)^2 \frac{j_l(\rho_a)(\rho_a j_l(\rho_a))' h_l(\rho_b)(\rho_b h_l(\rho_b))'}{\rho_a\rho_b}. \quad (56)$$

The right-hand side in eq. (56) is of order α^2, so that the frequency shift of a given resonance from $\theta_0 = 0$ is also of order α^2.

The dipole radiation is characterized by the extinction rate, which is the total energy emitted from the dipole per unit time interval. This quantity is evaluated as

$$ER(\omega) = ER^0(\omega)\Re[\sqrt{\epsilon_a}] + \frac{\omega}{2}\Im[\boldsymbol{d}^* \cdot \boldsymbol{E}^{aj}(\boldsymbol{x}_0)], \quad (57)$$

$$ER^0(\omega) = \frac{\mu_0\omega^4|\boldsymbol{d}|^2}{12\pi c}. \quad (58)$$

Here, $ER^0(\omega)$ is the extinction rate of the dipole in vacuum. Again, we have the factor $j_l(q_a r_0)$ in eq. (57) [see eqs. (37) and (38)]. Therefore, at $q_a r_0 = j_{l+\frac{1}{2},n}$, the possible enhancement of ψ^{Maj} is hidden. However, through the cross term of the polarization in the S-matrix, the resonance becomes visible through the $\beta = N$ channel.

Figure 4 shows the normalized extinction rate of a dipole placed inside an axionic sphere. The dipole position is chosen such that $q_a r_0 = j_{5+\frac{1}{2},1}$ is satisfied around the relevant resonance frequency. We can see that at $\theta_0 = \pi$, the resonance becomes visible, whereas the resonance is completely hidden at $\theta_0 = 0$. The extinction spectrum changes by more than 45% at the resonance frequency, otherwise it changes very little and is of order α^2. Therefore, the θ term can very strongly modulate the dipole radiation at resonance frequencies. We should note that a similar phenomenon can take place for magnetic dipole radiation by interchanging the roles of M and N polarizations.

From an experimental viewpoint, a dipole placed inside a

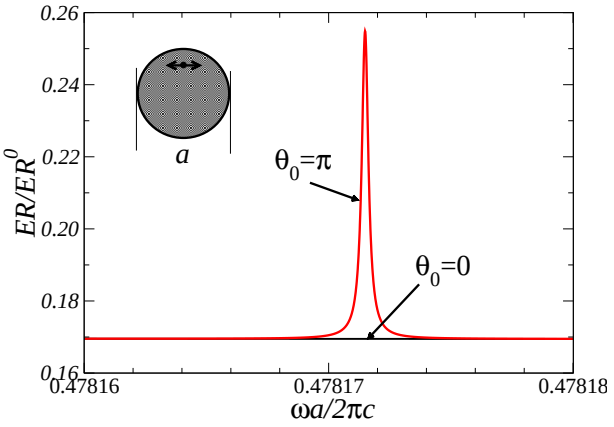

Fig. 4. (Color online) Extinction rate of an oscillating dipole inside a sphere of permittivity $\epsilon_a = 100$ and diameter a. Both normal ($\theta_0 = 0$) and axionic ($\theta_0 = \pi$) spheres are considered. A dipole whose moment is parallel to the sphere surface is placed at $r = r_d$, depending on its oscillation frequency in such a way that $q_a r_d = j_{5+\frac{1}{2},1} \simeq 9.356$ around the frequency of the third Mie resonance of M polarization with angular momentum $l = 5$.

sphere can be realized by embedding a light emitter, such as a quantum dot or dye molecule, having an electric-dipole transition. The extinction rate of the dipole is proportional to the decay rate or the inverse lifetime of the emitter via Fermi's golden rule. Therefore, the strong perturbation of the extinction rate can be observed experimentally via a lifetime measurement. To observe the clear contrast as shown in Fig. 4, the rotational symmetry of the specimen is crucial. If it is broken, M and N polarizations are no longer decoupled at $\theta_0 = 0$, giving rise to a possible peak of the extinction rate even at $\theta_0 = 0$. This will make the contrast of ER between $\theta = 0$ and π smaller. A numerical demonstration of such an effect is beyond the scope of the present paper.

6. Summary and Discussion

We have presented a theory of light scattering in axion electrodynamics. The S-matrix is derived analytically for planar, cylindrical, and spherical objects. Using the S-matrix, enhanced Faraday rotation, parity-violating light scattering, and strong perturbation in dipole radiation are demonstrated. These optical phenomena can be used to study a topological insulator optically.

Several points remain to be noted. An important issue is the relevance to chirality. Faraday rotation without a magnetic field, discussed in this paper, is reminiscent of the so-called Drude-Born-Fedorov (DBF) chirality:

$$\boldsymbol{D} = \epsilon_0\epsilon(\boldsymbol{E} + \beta\boldsymbol{\nabla}\times\boldsymbol{E}), \tag{59}$$

$$\boldsymbol{B} = \mu_0\mu(\boldsymbol{H} + \beta\boldsymbol{\nabla}\times\boldsymbol{H}). \tag{60}$$

Assuming a steady state of frequency ω, eqs. (59) and (60) become

$$\boldsymbol{D} = \epsilon_0\epsilon\boldsymbol{E} + \mathrm{i}\chi_c\boldsymbol{B}, \tag{61}$$

$$\boldsymbol{H} = \frac{1-\frac{\omega^2}{c^2}\epsilon\mu\beta^2}{\mu_0\mu}\boldsymbol{B} + \mathrm{i}\chi_c\boldsymbol{E}, \tag{62}$$

with $\chi_c = \epsilon_0\epsilon\beta\omega$. Therefore, magnetoelectric coupling takes place at nonzero frequencies. The dispersion relation in a homogeneous DBF medium is given by

$$k = \frac{\frac{\omega}{c}\sqrt{\epsilon\mu}}{1 \pm \frac{\omega}{c}\sqrt{\epsilon\mu}\beta}, \tag{63}$$

and the corresponding two eigenstates are left and right circular-polarized light. The time-reversal symmetry is preserved if ϵ, μ, and β are real, whereas the space-inversion symmetry is broken.

On the other hand, the constitutive relation in axion electrodynamics becomes

$$\boldsymbol{D} = \epsilon_0\epsilon\boldsymbol{E} + \chi_a\boldsymbol{B}, \tag{64}$$

$$\boldsymbol{H} = \frac{1}{\mu_0\mu}\boldsymbol{B} - \chi_a\boldsymbol{E}, \tag{65}$$

with $\chi_a = c\epsilon_0\alpha\theta/\pi$. Therefore, the magnetoelectric coupling emerges even at the static limit ($\omega = 0$), but the effect is topological. This is because the dispersion relation is the same as that in an ordinary medium, $k = (\omega/c)\sqrt{\epsilon\mu}$, and the effect arises only through the boundary as presented in the paper. At a generic value of θ, both the time-reversal and space-inversion symmetries are broken. Therefore, axion electrodynamics is completely different from the DBF chirality, although they both possess optical activity. For comparison, in multiferroic materials, magnetoelectric coupling also emerges. The coupling generally has an off-diagonal form and is given by the effective Lagrangian of $\Delta\mathcal{L} \propto \alpha_{ij}E_iB_j$. The dispersion relation is also altered from the ordinary relation. We also note that in the field of electromagnetic engineering the axionic medium is called the Tellegen medium and has been studied theoretically as a part of bi-isotropic media.[14,15] Recent investigation of metamaterial also sheds light on the Tellegen medium.[16]

Another important issue is the validity of the Lagrangian of eq. (1). In this paper we simply assume that eq. (1) can be applied in entire space-time for both axionic ($\theta \neq 0$) and non-axionic ($\theta = 0$) substances. The difference of axion electrodynamics from ordinary electrodynamics lies in the boundary condition of the surface Hall current presented in §2. One may wonder whether such a boundary condition correctly takes account of the surface states of a topological insulator, which is a representative axionic substance.

Concerning this issue, we implicitly assume that a small gap ΔE_s in the surface states opens by some means (e.g., by attaching a thin magnetic layer to the surface) and that the operating frequencies of the radiation field under study are below the gap energy, $\omega < \Delta E_s/\hbar$. Under this condition, the effective theory of the radiation field is well-defined in the following sense. The Lagrangian of eq. (1) is to be derived by integrating out the matter fields in the bulk topological insulator. If there is a gapless surface state, the integration will have the infrared divergence, which may affect some physical properties. However, if there is a gap, the integration will be well-defined.

We also note that the 3+1-dimensional (d) Lagrangian of eq. (1) is gauge-invariant, regardless of the geometry of the 3d topological insulator. This gauge invariance provides a striking contrast to the broken gauge invariance of the 2+1d Chern-Simons Lagrangian for a 2d quantum Hall system,

$$\mathcal{L}_{\mathrm{CS}} = \frac{\sigma_H}{2}\epsilon^{\mu\nu\rho}A_\mu\partial_\nu A_\rho, \tag{66}$$

provided the 2d system has open boundaries. Here, σ_H is the 2d Hall conductivity, $\epsilon^{\mu\nu\rho}$ is the totally antisymmetric tensor with $\epsilon^{012} = 1$, and A_μ is the gauge field. The Chern-Simons Lagrangian is also derived by integrating out matter fields of the 2d quantum Hall system. In this case, to compensate the broken gauge invariance, an additional term in the effective Lagrangian is needed, giving rise to an additional current localized near the edge.[17,18] Therefore, from the viewpoint of gauge invariance, we may regard eq. (1) as the effective Lagrangian irrespective of the geometry of the topological insulator, although the addition of a surface-localized gauge-invariant effective Lagrangian is still allowed.

In a topological insulator, the spin-orbit interaction plays a crucial role. It is interesting to note that the (electronic) spin-orbit interaction results in the θ term in the effective Lagrangian of the radiation field, and that the θ term induces a new class of the photospin-orbit interaction. Whether or not this interaction gives rise to a photonic counterpart of a topological insulator is an important issue. In this context a recent investigation of a photonic topological insulator[19] may be instructive.

In this paper we have concentrated on static and piecewise-constant axion fields. If a time-dependent θ is available, there will be a frequency shift for an incident monochromatic wave. For instance, if the axion field jumps to 0 in a certain switching time, the frequency shift will be on the order of the inverse switching time. Moreover, the effect of a spatially varying axion field is an important issue. This problem is closely related to the search for axions in particle physics.[20] A popular method of searching for axions is to use the Primakoff effect,[21,22] which results in the conversion of a photon to an axion under a strong external field. This effect combined with multiple scattering in an ensemble of nonaxionic scattering objects may enhance the interaction between an axion and photon, resulting in an improvement of axion detection efficiency.

We hope this paper will stimulate further investigation of axion electrodynamics from various points of view.

Acknowledgments

The author would like to thank Prof. H. Miyazaki and Dr. N. Maeda for valuable discussions. This work was supported by KAKENHI (Grant No. 23540380) of Japan Society for the Promotion of Science.

Appendix

In the appendix we summarize the vector spherical expansion coefficients. The coefficients $\boldsymbol{P}^\beta$ are defined by

$$\mathrm{i}\boldsymbol{L}\psi(\boldsymbol{x}) = \sum_{LL'} z_l(qr)Y_L(\hat{\boldsymbol{x}})[\boldsymbol{P}^M]_{LL'}\psi_{L'}, \tag{A·1}$$

$$\frac{1}{q}\boldsymbol{\nabla}\times\mathrm{i}\boldsymbol{L}\psi(\boldsymbol{x}) = \sum_{LL'} z_l(qr)Y_L(\hat{\boldsymbol{x}})[\boldsymbol{P}^N]_{LL'}\psi_{L'}, \tag{A·2}$$

$$\psi(\boldsymbol{x}) = \sum_{L} z_l(qr)Y_L(\hat{\boldsymbol{x}})\psi_L, \tag{A·3}$$

where z_l is either the spherical Bessel or spherical Hankel function of order l. If we define the spherical harmonics as

$$Y_L(\hat{\boldsymbol{x}}) = (-1)^{\frac{m+|m|}{2}}\sqrt{\frac{2l+1}{4\pi}\frac{(l-|m|)!}{(l+|m|)!}}\mathrm{e}^{\mathrm{i}m\phi}P_l^{|m|}(\cos\theta), \tag{A·4}$$

then we obtain

$$[P_x^M]_{LL'} = \mathrm{i}A^L_{0+}\delta_{L',L_{0+}} + \mathrm{i}A^L_{0-}\delta_{L',L_{0-}}, \tag{A·5}$$

$$[P_y^M]_{LL'} = -A^L_{0+}\delta_{L',L_{0+}} + A^L_{0-}\delta_{L',L_{0-}}, \tag{A·6}$$

$$[P_z^M]_{LL'} = \mathrm{i}m\delta_{L',L}, \tag{A·7}$$

$$[P_x^N]_{LL'} = (l+2)B^L_{++}\delta_{L',L_{++}} - (l+2)B^L_{+-}\delta_{L',L_{+-}} - (l-1)B^L_{-+}\delta_{L',L_{-+}} + (l-1)B^L_{--}\delta_{L',L_{--}} \tag{A·8}$$

$$[P_y^N]_{LL'} = \mathrm{i}(l+2)B^L_{++}\delta_{L',L_{++}} + \mathrm{i}(l+2)B^L_{+-}\delta_{L',L_{+-}} - \mathrm{i}(l-1)B^L_{-+}\delta_{L',L_{-+}} - \mathrm{i}(l-1)B^L_{--}\delta_{L',L_{--}} \tag{A·9}$$

$$[P_z^N]_{LL'} = -(l+2)C^L_{+0}\delta_{L',L_{+0}} - (l-1)C^L_{-0}\delta_{L',L_{-0}}, \tag{A·10}$$

$$A^L_{0\pm} = \frac{1}{2}\sqrt{(l\mp m)(l\pm m+1)}, \tag{A·11}$$

$$B^L_{+\pm} = \frac{1}{2}\sqrt{\frac{(l\pm m+1)(l\pm m+2)}{(2l+1)(2l+3)}}, \tag{A·12}$$

$$B^L_{-\pm} = \frac{1}{2}\sqrt{\frac{(l\mp m-1)(l\mp m)}{(2l-1)(2l+1)}}, \tag{A·13}$$

$$C^L_{+0} = \sqrt{\frac{(l+m+1)(l-m+1)}{(2l+1)(2l+3)}}, \tag{A·14}$$

$$C^L_{-0} = \sqrt{\frac{(l+m)(l-m)}{(2l-1)(2l+1)}}, \tag{A·15}$$

$$L_{0\pm} = (l, m\pm 1),\ L_{\pm 0} = (l\pm 1, m),$$
$$L_{\pm+} = (l\pm 1, m+1),\ L_{\pm-} = (l\pm 1, m-1). \tag{A·16}$$

The M and N polarizations are orthogonal in the sense that

$$[(\boldsymbol{P}^\beta)^\dagger\cdot\boldsymbol{P}^{\beta'}]_{LL'} = l(l+1)\delta_{L,L'}\delta_{\beta,\beta'}. \tag{A·17}$$

1) R. D. Peccei and H. R. Quinn: Phys. Rev. Lett. **38** (1977) 1440.
2) R. Bradley, J. Clarke, D. Kinion, L. J. Rosenberg, K. van Bibber, S. Matsuki, M. Mück, and P. Sikivie: Rev. Mod. Phys. **75** (2003) 777.
3) X.-L. Qi, T. L. Hughes, and S.-C. Zhang: Phys. Rev. B **78** (2008) 195424.
4) F. Wilczek: Phys. Rev. Lett. **58** (1987) 1799.
5) J. Maciejko, X.-L. Qi, H. D. Drew, and S.-C. Zhang: Phys. Rev. Lett. **105** (2010) 166803.
6) A. M. Essin, J. E. Moore, and D. Vanderbilt: Phys. Rev. Lett. **102** (2009) 146805.
7) A. Karch: Phys. Rev. B **83** (2011) 245432.
8) W.-K. Tse and A. H. MacDonald: Phys. Rev. Lett. **105** (2010) 057401.
9) F. Jonsson and C. Flytzanis: Phys. Rev. Lett. **97** (2006) 193903.
10) J. B. Pendry: *Low Energy Electron Diffraction* (Academic, London, 1974).
11) K. Ohtaka, T. Ueta, and K. Amemiya: Phys. Rev. B **57** (1998) 2550.
12) J. Stratton: *Electromagnetic Theory* (McGraw-Hill, New York, 1941).
13) K. Ohtaka and Y. Tanabe: J. Phys. Soc. Jpn. **65** (1996) 2265.
14) B. Tellegen: Philips Res. Rep **3** (1948) 81.
15) I. V. Lindell, A. H. Sihvola, S. A. Tretyakov, and A. J. Viitanen: *Electromagnetic waves in chiral and bi-isotropic media* (Artech House, Norwood, 1994).
16) A. Sihvola and S. Zouhdi: in*Metamaterials and Plasmonics: Fundamentals, Modelling, Applications*, ed. S. Zouhdi, A. Sihvola, and A. P. Vinogradov (Springer, Netherlands, 2009), p. 3.
17) X. G. Wen: Phys. Rev. B **43** (1991) 11025.
18) N. Maeda: Phys. Lett. B **376** (1996) 142.

19) V. Yannopapas: Phys. Rev. B **84** (2011) 195126.
20) P. Sikivie, D. B. Tanner, and K. van Bibber: Phys. Rev. Lett. **98** (2007) 172002.
21) H. Primakoff: Phys. Rev. **81** (1951) 899.
22) F. T. Avignone, D. Abriola, R. L. Brodzinski, J. I. Collar, R. J. Creswick, D. E. DiGregorio, H. A. Farach, A. O. Gattone, C. K. Guérard, F. Hasenbalg, H. Huck, H. S. Miley, A. Morales, J. Morales, S. Nussinov, A. Ortiz de Solórzano, J. H. Reeves, J. A. Villar, and K. Zioutas: Phys. Rev. Lett. **81** (1998) 5068.